Pseudocontinuum Polarimetry with the GBT

Brian S. Mason
v.1 31may07
v.2 03sep07

Abstract

We outline a simple method for calibrating correlation polarimetric data from the GBT spectrometer, and describe its application to a deep continuum project. We quantify the noise performance of the system in total intensity and polarization, finding that the system noise is a factor of $50 - 100$ above the radiometer equation in Stokes I, but only a factor of ~ 4 above it in Q and U, although times when radiometric performance is achieved are seen and there so there is a significant variation with observing epoch. We note the existence of a $\sim 10\%$ Q,U residual to our calibration which is a function of parallactic angle. We comment on prospects for the method.

1 Introduction

The technique of single-dish correlation polarimetry has been developed by Carl Heiles and collaborators, and was mainly motivated by studies of circularly polarized Zeeman line radiation. At the frequencies of interest for the Zeeman measurements most receivers intrinsically measure linear polarization; in this case the highly stable cross-correlation products measure the circular polarization V and one of the linearly polarized stokes parameters, which one depending on the angle of the feeds with respect to the sky.

The stability advantages offered by nulling the total power by cross-correlation are also of interest to those seeking to make broadband continuum measurements, where DC stability is always the first concern. Most continuum radiation is linearly polarized; the motivation of this work to develop the capability to measure the polarization of CMB foregrounds at 8 GHz and up. At these frequencies all of the GBT receivers measure native circular polarization, which is ideal as both of the Stokes linear polarization parameters (Q, U) should then be minimally affected by gain fluctuations and variations in the emission of the atmosphere.

In this memo we describe our approach to calibrating weakly polarized psuedocontinuum data and present some results from the telescope.

2 Mueller Matrices

We adopt the basic terminology of Heiles et al. to describe the celestial-to-nominal Stokes transfer equations:

$$M_{tot} = M_A \, X \, M_{IF} \, M_F \, M_{sky} \tag{1}$$

Here M_A describes the gain and phase response of the electronics; M_{IF} describes the feed cross-polarization response; M_F describes the basic feed response; and M_{sky} enacts the rotation of the sky. All are 4×4 matrices, ultimately relating true on-sky Stokes parameters to a combination of the measured cross-correlations, by:

$$S_{out} = M_{tot} S_{in} \tag{2}$$

We consider only the case of native circular feeds. X is a change-of-basis transformation we introduce, discussed below.

3 The Basic Scheme

We have adopted a slightly different approach to the calibration than Heiles et al. This was motivated by two considerations. First, in order to minimize the loss of coherence in the continuum average it was desirable to model the variation in the phase of the correlation as a function of frequency carefully; as a corrolarry to this, while not strictly required, it seemed worthwhile to measure the S_{cal} explicitly as a function of frequency and make use of the information. Second, to simplify and expedite the fitting, we sought a linear data model. The cost of these simplifications is that the instrument model is entirely phenomenological.

Rearranging eq. 1, we have

$$X^{-1}\, M_A^{-1}\, S_{out} = S'_{out} = M_{IF}\, M_F\, M_{sky}\, S_{in} \tag{3}$$

We *define* M_A as an approximate celestial calibration relating raw counts to Janskys or Kelvin, and assume that all of the frequency dependence of our calibration within one IF is contained in this factor. This basic factorization defines our approach: M_A will be determined from observations of an effectively unpolarized celestial calibrator plus the correlated cal, and a lumped $M_{IF} M_F M_{sky}$ response will be determined from observations of a polarized calibrator. The treatment is simple if at first we order the raw correlator outputs as

$$S_{out} = \begin{pmatrix} LL \\ LR \\ RL \\ RR \end{pmatrix} \tag{4}$$

which motivates our introduction of the change-of-basis transformation

$$X^{-1} = \begin{pmatrix} 1 & 0 & 0 & 1 \\ 0 & 1 & 0 & 0 \\ 0 & 0 & -1 & 0 \\ 1 & 0 & 0 & -1 \end{pmatrix} \tag{5}$$

We rewrite eq. 3 as

$$X^{-1}\, M_A^{-1}\, S_{out} = S'_{out} = M_T\;\, M_{sky}\, S_{in} \tag{6}$$

Here we have introduced S'_{out}, a reordered version of S_{out}, which heuristically is

$$S'_{out} = \begin{pmatrix} LL+RR \\ Im(LR) \\ -Re(LR) \\ LL-RR \end{pmatrix} = \begin{pmatrix} LL+RR \\ LR \\ -RL \\ LL-RR \end{pmatrix} \tag{7}$$

which is equal to $(I,Q,U,V)^T$ for a perfect system at zero rotation. S'_{out} has been phase and amplitude calibrated by a procedure we will describe, and thus has units of Janskys or Kelvin; we will refer to it as the "nominal" Stokes vector. X^{-1} is the matrix which effects the reordering

M_T is the lumped polarization transfer response of the telescope plus feeds (everything before the point of injection of the correlated cal signal)

$$M_T = \begin{pmatrix} m_{ii} & m_{iq} & m_{iu} & m_{iv} \\ m_{qi} & m_{qq} & m_{qu} & m_{qv} \\ m_{ui} & m_{uq} & m_{uu} & m_{uv} \\ m_{vi} & m_{vq} & m_{vu} & m_{vv} \end{pmatrix} \tag{8}$$

We will explicitly solve for the matrix elements m from observations of the polarization calibrator.

3.1 Phase and Amplitude Calibration

We assume that the dominant effects in the data are electronic gains and phase differences between the individual L and R channels. This implies that M_A will have the form:

$$M_A(f) = \begin{pmatrix} G_L(f) & 0 & 0 & 0 \\ 0 & \sqrt{G_L(f)G_R(f)}\,cos\,\psi(f) & \sqrt{G_L(f)G_R(f)}\,sin\,\psi(f) & 0 \\ 0 & -\sqrt{G_L(f)G_R(f)}\,sin\,\psi(f) & \sqrt{G_L(f)G_R(f)}\,cos\,\psi(f) & 0 \\ 0 & 0 & 0 & G_R(f) \end{pmatrix} \tag{9}$$

G_L and G_R are the total intensity gains of the system (counts/Jy), and $\psi(f)$ is the phase of the correlated cal signal. These are determined as

$$G_L(f) = \frac{LL_{cal\,on}(f) - LL_{cal\,off}(f)}{S_{cal,L}(f)} \tag{10}$$

where S_{cal} is nominally determined from an independent set of observations

$$S_{cal,L} = \frac{LL_{cal\,on}(f) - LL_{cal\,off}(f)}{LL_{on\,src}(f) - LL_{off\,src}(f)}\,S_{src}(f) \tag{11}$$

and similarly for RR.

The phase is determined as

$$\psi(f) = Atan\left(\frac{RL_{cal\,on}(f) - RL_{cal\,off}(f)}{LR_{cal\,on}(f) - LR_{cal\,off}(f)}\right) \tag{12}$$

The dominant effect is a path length difference of about 60 cm. However we found significant ($\pm 15°$ or sometimes greater) residuals to this linear phase gradient and deemed it best to explicitly compute & apply the phase as a function of frequency.

After applying this calibration we replace the spectra with their averages over frequency.

3.2 Polarization Calibration

With the instrumental phase corrected, we can use observations of a point source of known polarization to determine the polarization response of the instrument. This requires a number $j = 1 ... N_{obs}$ of independent observations at a range of parallactic angles. For a single observation $S'_{out,j}$ (with phase and amplitude corrections having been applied as described in § 3.1), we have

$$S'_{out,j} = M_T \, M_{sky}(PA_j) \begin{pmatrix} I \\ Q \\ U \\ V \end{pmatrix} \tag{13}$$

where I, Q, U, and V are the known stokes parameters of the polarization calibrator.

For a single observation j, we re-arrange Eq. 13 as

$$S'_{out,j} = \left(\begin{matrix} I & c_jQ + s_jU & -s_jQ + c_jU & 0 & 0 & 0 \\ 0 & 0 & 0 & I & c_jQ + s_jU & -s_jQ + c_jU \\ 0 & 0 & 0 & 0 & 0 & 0 \\ 0 & 0 & 0 & 0 & 0 & 0 \end{matrix} \right. \; ... \tag{14}$$

$$... \left. \begin{matrix} 0 & 0 & 0 & 0 & 0 & 0 \\ 0 & 0 & 0 & 0 & 0 & 0 \\ I & c_jQ + s_jU & -s_jQ + c_jU & 0 & 0 & 0 \\ 0 & 0 & 0 & I & c_jQ + s_jU & -s_jQ + c_jU \end{matrix} \right) \begin{pmatrix} m_{ii} \\ m_{iq} \\ m_{iu} \\ m_{qi} \\ m_{qq} \\ m_{iu} \\ m_{ui} \\ m_{uq} \\ m_{uu} \\ m_{vi} \\ m_{vq} \\ m_{vu} \end{pmatrix}$$

where we have used the shorthand $c_j = cos(2PA_j)$, $s_j = sin(2PA_j)$ for the sky rotation factors. Stokes V for the calibrator source is assumed to be zero, so matrix elements connecting true V to nominal Stokes parameters are unconstrained[1] This is a 4×12 matrix: no unique solution exists for a single

[1] In subsequent matrix manipulations one should set $m_{vv} = 1.0$ or some other finite value comparable to other matrix elements, so that the matrices are stable. Setting the entire V column to zero, for instance, is a bad idea.

observation. By stacking expression 14 for multiple observations at a range of parallactic angles one obtains a $4N_{obs} \times 12$ matrix. In principle then, for only 3 observations the full Mueller matrix can be solved for with standard linear least squares techniques.

Once the Mueller matrix is in hand, observations of other targets may be calibrated as

$$S_{true} = (M_T\, M_{sky})^{-1} S'_{out} = (M_T\, M_{sky})^{-1}\, X^{-1}\, M_A^{-1} S_{out} \tag{15}$$

3.3 Jones-matrix Approach

Another approach, as described by Heiles et al., is to write the Mueller matrices in terms of a set of physical, parametric Jones matrices and to fit for these model parameters from the polarization calibrator data. This approach has the advantage of automatically including the constraints implied by the symmetries of the problem, but the practical disadvantage that the fitting problem is then nonlinear and has a number of ambiguous phases. A preliminary comparison of these approaches on our data yields consistent results.

A more careful review of this comparison would be enlightening, as would a review of the IQU beammaps determined from our spider scans, the analysis of which is not discussed in this memo.

4 Application to X-band Data

In 11 runs totalling 46 hours from 21feb07 through 21mar07, we observed the dark cloud LDN1622, a known source of anomalous microwave emission in stokes I (project 7a30, investigators: Mason, Robishaw, & Finkbeiner). We used the X-band receiver with two 200 MHz IFs centered at 8.65 and 9.65 GHz, frequencies chosen to be local, smooth minima of T_{rx} and to have relatively little RFI based on site survey data. Every hour or so, we did a peak and focus on the fortuitously nearby polarization calibrator 3c138, and an On-Off observation of it with the spectrometer.

A summary of our data reduction pipeline is in the appendix.

4.1 RFI

Frequent narrowband RFI, sometimes strong, was seen in the 9.65 ± 0.1 GHz band, in spite of both bands having been chosen to be relatively RFI-free based on site monitor data (W. Sizemore, private communication). A few channel ranges were flagged in all observations; 5σ spikes in the uncalibrated LR and RL data were also sought automatically, and any integrations showing them excluded.

No significant RFI was found in the 8.65 ± 0.1 GHz band.

4.2 Phase and Amplitude Calibration

To give a sense of what the important effects in the data are, the following figures show some raw and calibrated data.

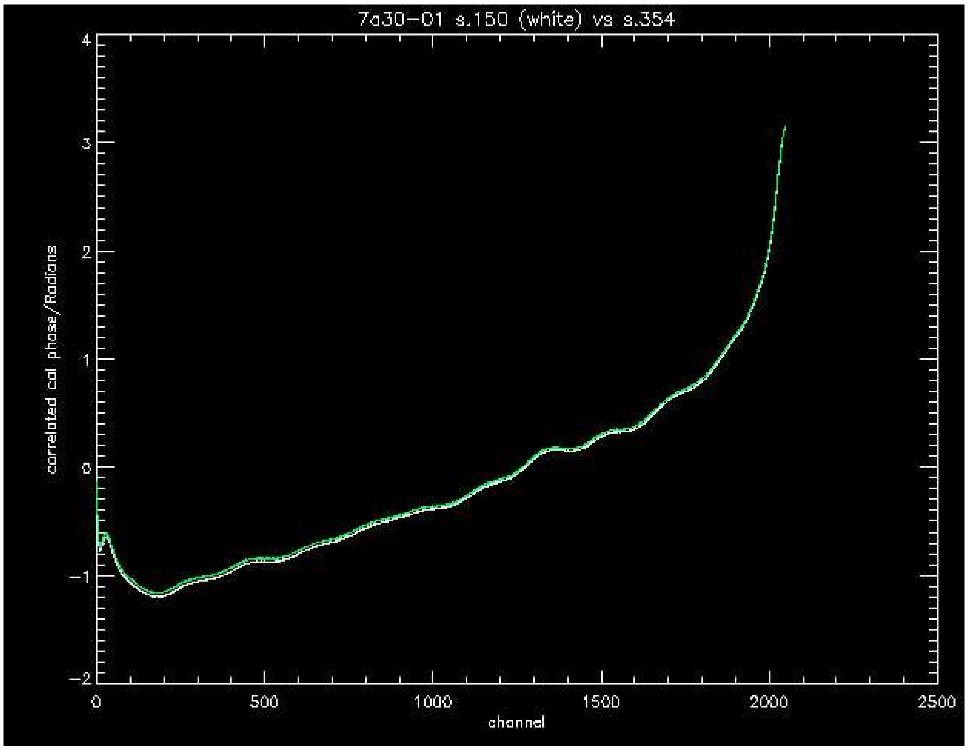

Figure 1: The phase stability was seen to be excellent over a single run, as illustrated by this comparison of the phase of the cal signal for scans 150 and 354 of project session 1.

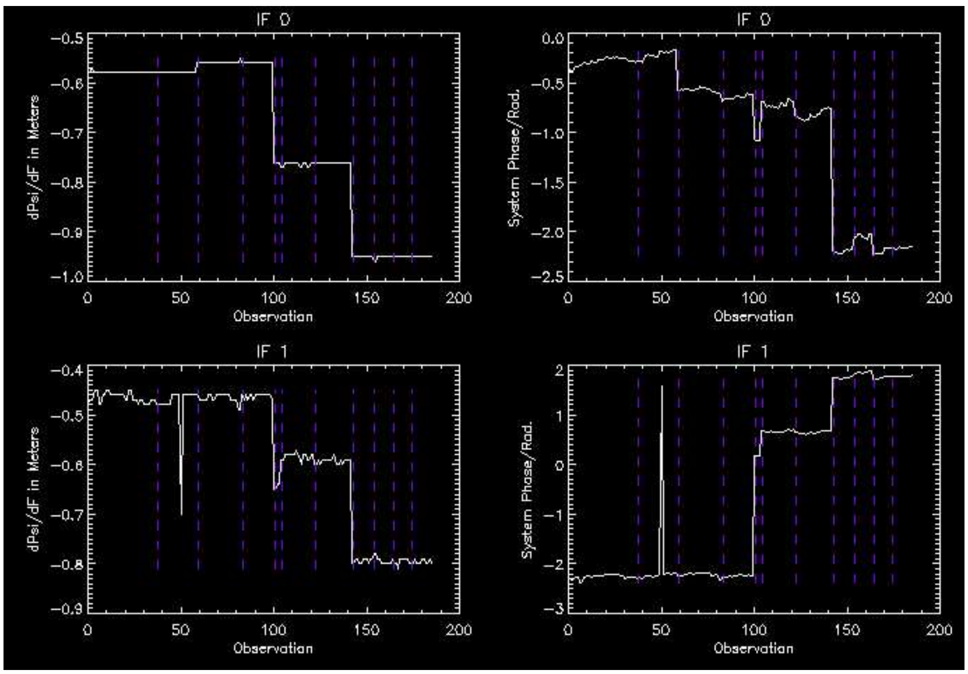

Figure 2: By fitting the phase to $\psi = \psi_0 + B(\nu - \nu_0)$ a a path length difference between the L and R polarization signals can be determined. This figure shows the results for the system phase ψ_0 and the path length difference obtained from fits to all the scans with the cal diode on. Vertical, dashed purple lines separate observing runs. The runs take place over a total time span of about 1 month. Receiver work at the IF outputs was done after the 4th run.

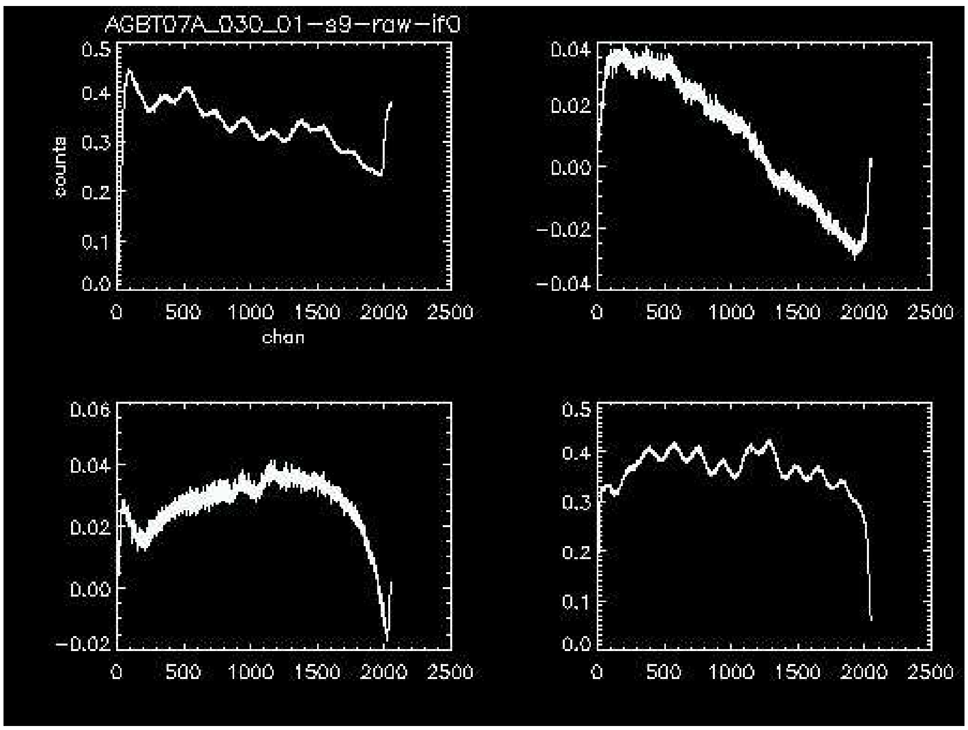

Figure 3: Raw LL, LR, RL, and RR spectra for one On-Off observation of 3c138. The x-axis is channel number; the total bandwidth displayed is 200 MHz.

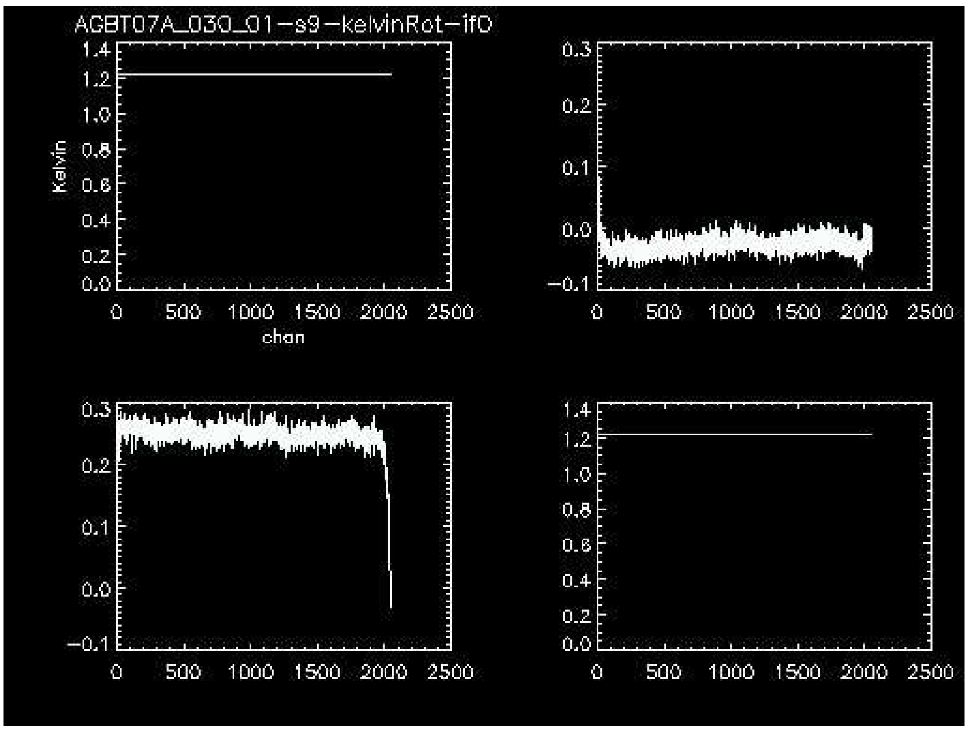

Figure 4: Phase and amplitude calibrated LL, LR, RL, and RR data. Note that LL and RR each show half of the stokes I signal. The x-axis is channel number; the total bandwidth displayed is 200 MHz.

4.3 Calibration on 3c138

All observations of 3c138, from all 11 observing sessions, were phase and amplitude calibrated to obtain nominal stokes, shown in Figure 4.3 as a function of parallactic angle.

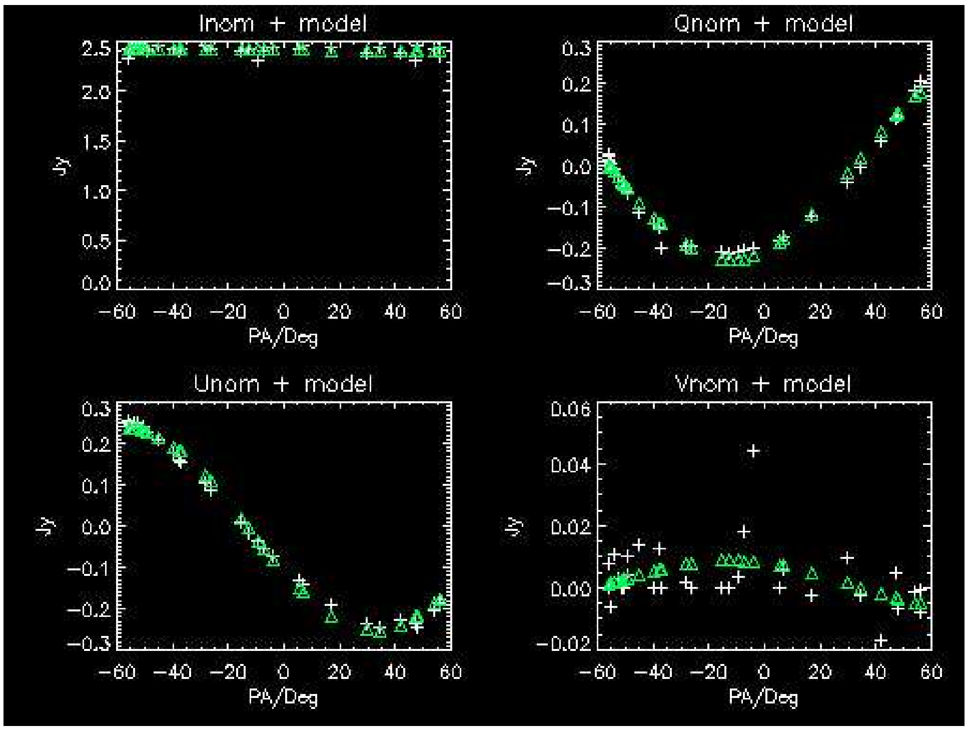

Figure 5: Nominal I, Q, U, & V for all On-Off observations of 3c138. Data are in white, the best-fit model is shown by green triangles.

The Mueller matrix M_T obtained for IF0 (8.65 GHz) is

$$M_T(8.65\,GHz) = \begin{pmatrix} 0.993246 & 0.0378273 & 0.0291846 & 0.00000 \\ 0.00355346 & -0.885070 & -0.0651197 & 0.00000 \\ -0.00305395 & -0.0817768 & 0.914964 & 0.00000 \\ 0.000360488 & 0.0300088 & 0.00304029 & 1.00000 \end{pmatrix} \tag{16}$$

The Mueller matrix for IF1 (9.65 GHz) is

$$M_T(9.65\,GHz) = \begin{pmatrix} 0.992025 & 0.0395148 & 0.0372477 & 0.00000 \\ -0.00658511 & -0.769852 & 0.268332 & 0.00000 \\ -0.00113739 & 0.234783 & 0.795728 & 0.00000 \\ -0.00548045 & 0.0188669 & 0.0654412 & 1.00000 \end{pmatrix} \tag{17}$$

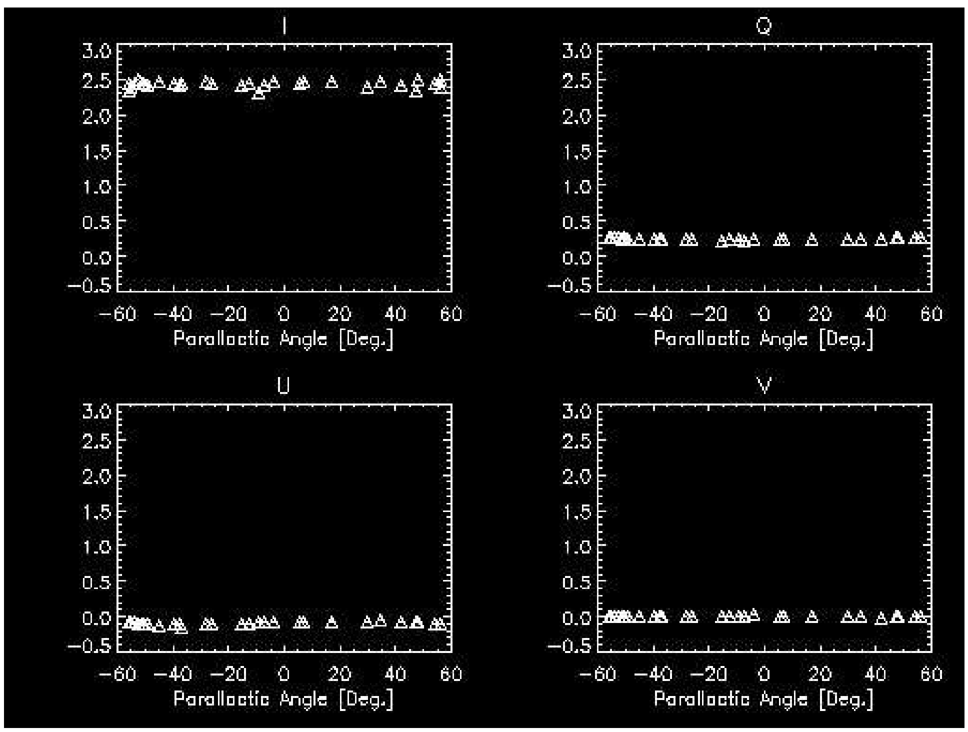

Figure 6: Fully calibrated 3c138 data (IF0)

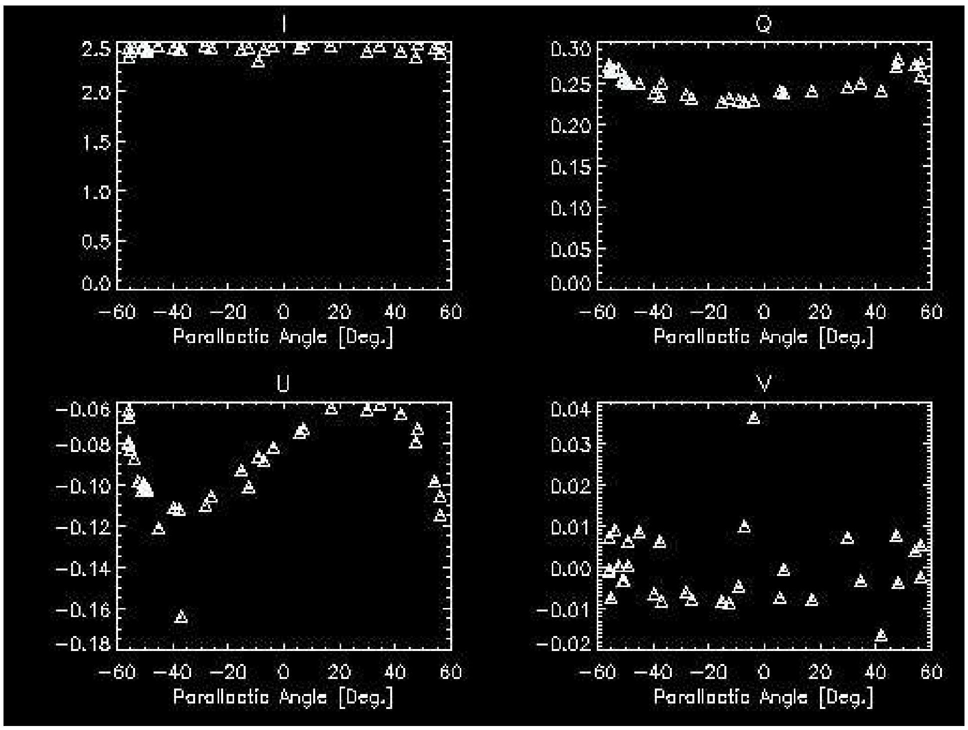

Figure 7: Fully calibrated 3c138 data (IF0) on a scale that better shows the parallactic-angle dependent residuals to the calibration. Similar residuals are seen in the independent IF1 calibration, and in independent analyses of different X-band datasets by Carl Heiles & Tim Robishaw.

4.4 Best-current Results & Broadband Continuum Performance

We use our 36 hours of good data on LDN1622 to characterize the broadband continuum performance of the system. Observations comprised successive On-Off observations, with 38 seconds of integration in each phase. The expected stokes I continuum is about a millikelvin, so effectively these are blank-sky observations. The noise was evaluated by comupting the median absolute deviation of fully calibrated On-Off observations in half-hour sliding buffers; the results for all 732 nominally useful observations are shown in Figure 4.4. The median absolute deviation is an estimator of the width of the core of the noise distribution which is less sensitive to outliers than the root mean square. Here it is normalized to equal the RMS if the distribution is Gaussian.

The expected noise in these measurements is roughly

$$\sigma = \frac{\sqrt{2}}{2\,K/Jy}\,\frac{27\,K}{\sqrt{200\times 10^{6}\,Hz\ \times 38\,sec}} = 0.2\,mJy \tag{18}$$

Our final, fully averaged result has a sensitivity (assume $2\,K/Jy$ and a main beam efficiency of 78%) of about $63\,\mu K$ at 8.65 GHz and $41\,\mu K$ at 9.65 GHz. Combining them together yields $34\,\mu K$ RMS. How does this compare with our goal of $7\,\mu K$ RMS in antenna (should be main-beam) temperature? From Figure 4.4 we see that stokes Q and U typically run a factor of 1.4 to 5 or so over theoretical; $34/4/sqrt2 = 6\,\mu K$, which is in agreement.

5 Conclusions & Prospects

The scatter in the Q & U data is typically less than that in stokes I by a factor of 25 or more, demonstrating the advantage of the cross-correlation technique to measure linearly polarized continuum. It is still at times a factor of 5 more than the radiometer equation's prediction, and fairly variable. This variation hasn't been found to correlate with any independent variable, e.g., the weather, and could be due to residual, low-level RFI in the data. Put another way, it is not clear why most of the time we do not achieve radiometer-equation limited performance in stokes Q & U. More investigation in this area is needed.

All GBT receivers above 6 GHz have native circular feeds so are suitable to be used to measure linear polarization using the approach outlined in this technical note. Presently only the X and Q band receivers (covering 8-12 and 40-48 GHz) have cal diode signals which are coherent between orthogonal polarizations of a given feed; in some cases this could be changed without removing the receiver from the telescope. Since essentially all GBT observations are done with both cal diodes firing simultaneously, there would be no loss in capability if all receivers had their cals reconnected so that the orthogonal polarizations were coherent. Given a sufficiently close, bright linear polarization calibrator on the sky, a coherent cal might be dispensed with in the meantime. At the frequencies of 12 GHz and up, it should also be possible to make full use of the

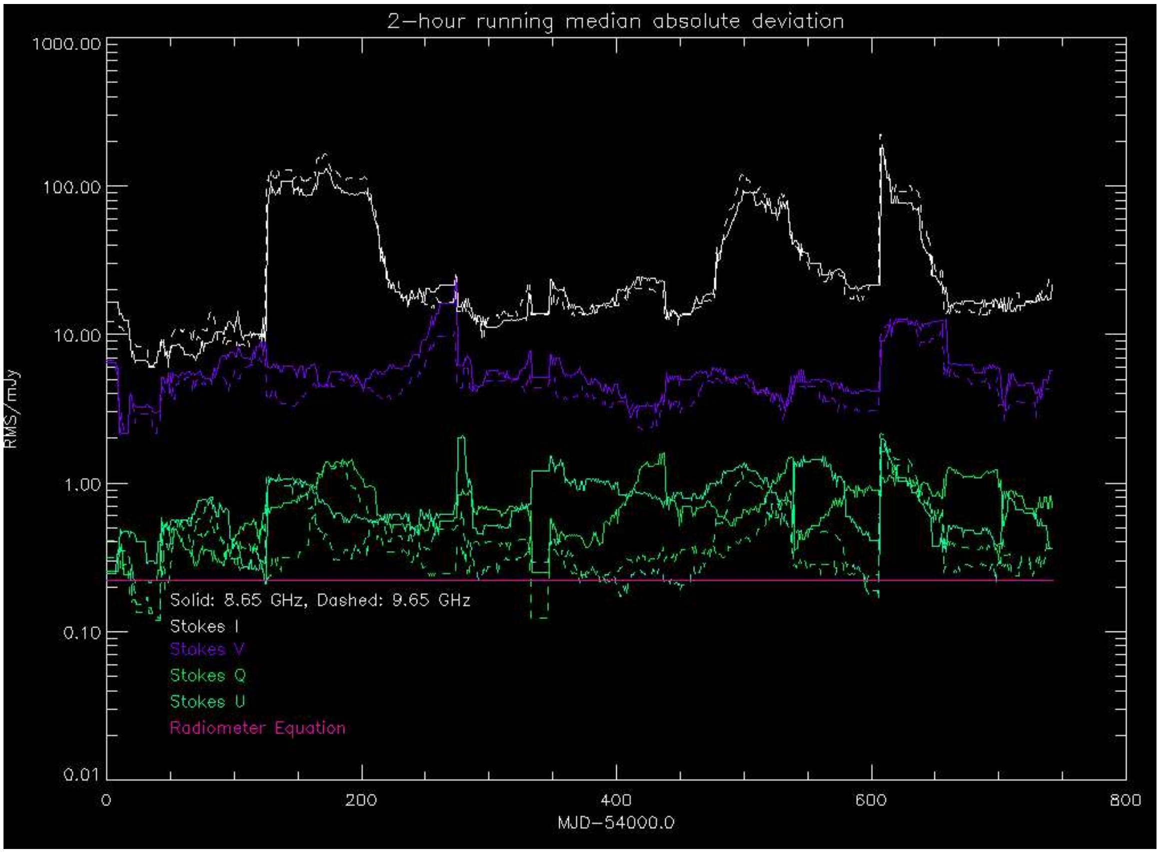

Figure 8: Median Absolute Deviation in mJy vs observation number for each stokes parameter in all 732 45-second On-Off observations of the target source LDN1622. Periods of enhanced scatter in Stokes I correspond to observing sessions with bad weather. Periods where stokes Q & U drop below the radiometer equation noise level are due to small number statistics (buffers with very few usable measurements). The reason for the factor of 4 variation in stokes Q & U noise levels is not known.

GBT spectrometer's 3.2 GHz bandwidth, instead of the 2×200 MHz used here (which was constrained mainly by RFI). Due to a combination of antenna gain, receiver temperature, and sky temperature, the GBT K and Ka band systems are a factor of at least 2.5 more sensitive than the Q-band system and would be preferred for most continuum polarization projects. The Ka-band system has the additional advantage of having the capability to perform sensitive (near radiometer-noise limited over 3.5 GHz) stokes I continuum measurements with the Caltech Continuum Backend.

The polarization capability of the GBT is of substantial interest for upcoming CMB polarization experiments and should be further developeod.

Acknowledgements: I thank my collaborators— Tim Robishaw, Doug Finkbeiner, Carl Heiles, & Tom Devlin— for useful comments and discussions; the GB electronics staff for diligent & careful support of the X-band receiver during our observing run; all those who worked on the GBT spectrometer over the years; & Carl Bignell for accomadating our sometimes difficult scheduling constraints.

Bibliography

Heiles, C. et al. 2001, PASP 113 1247

A Data Analysis Pipeline

The data analysis was done entirely within GBTIDL, a set of tools and routines provided by NRAO to facilitate reducing spectroscopic GBT data. Most of the needed operations did not exist so were added in as an extensive set of custom scripts developed specifically for psuedocontinuum cross-correlation data. These scripts would be easily applied to any GBT cross-correlation On-Off data, eg, collected at a different frequency with a different receiver.

1. Use GB's standard routine `SDFITS` to fill the data from each run from the raw engineering FITS files into a single

2. Flag scans in which the features in the cross-correlated spectra show peak values greater than 0.06 counts (about 5 times the thermal noise)

3. Phase and amplitude calibrate to nominal Q and U in Kelvin

4. Average over frequency to obtain continuum values for nominal I,Q,U,V

5. Apply Mueller Matrix

6. Compute median absolute deviation in a sliding 2 hours window, normalized to reproduce the RMS for a Gaussian distribution; use this as our error estimate for each On-Off measurement.

7. Reject individual On-Off integrations for which (using error estimates from the previous step) the data lie more than 4σ from the mean. Do this independently for each of $IQUV$.

8. Reject integrations at the center of buffers where the noise level was more than 5 x thermal in stokes Q & U, or more than 5x the minimum RMS in stokes I

9. Compute a weighted mean for the final answer.